AAC Accepted Manuscript Posted Online 11 June 2018
Antimicrob. Agents Chemother. doi:10.1128/AAC.00766-18

Orally Efficacious Broad-Spectrum Ribonucleoside Analog Inhibitor of Influenza and Respiratory Syncytial Viruses

Jeong-Joong Yoon[1#], Mart Toots[1#], Sujin Lee[2,3], Myung-Eun Lee[1], Barbara Ludeke[4], Jasmina M Luczo[5], Ketaki Ganti[6], Robert M Cox[1], Zachary M. Sticher[7], Vindya Edpuganti[7], Deborah. G. Mitchell[7], Mark A. Lockwood[7], Alexander A Kolykhalov[7], Alexander L Greninger[8], Martin L Moore[2,3], George R Painter[7], Anice C Lowen[6], Stephen M Tompkins[5], Rachel Fearns[4], Michael G Natchus[7], and Richard K Plemper[1,*]

[1]Institute for Biomedical Sciences, Georgia State University, Atlanta, GA
[2]Department of Pediatrics, Emory University School of Medicine, Atlanta, GA
[3]Children's Healthcare of Atlanta, Atlanta, GA
[4]Department of Microbiology, Boston University School of Medicine, Boston, MA
[5]Center for Vaccines and Immunology, University of Georgia, Athens, GA
[6]Department of Microbiology & Immunology, Emory University School of Medicine, Atlanta, GA
[7]Emory Institute for Drug Development, Emory University, Atlanta, GA
[8]Virology Division, Department of Laboratory Medicine, University of Washington, Seattle, WA

Running Title: Inhibitor of influenza-like diseases

[#]These authors contributed equally to the study

*Address correspondence to Richard K. Plemper, rplemper@gsu.edu

Abstract

Morbidity and mortality resulting from influenza-like disease are a threat especially for older adults. To improve case management, next-generation broad-spectrum antiviral therapeutics are urgently needed that are efficacious against major drivers of influenza-like disease including influenza viruses and respiratory syncytial virus (RSV). Using a dual-pathogen high throughput screening protocol for influenza A virus (IAV) and RSV inhibitors, we have identified N^4-hydroxycytidine (NHC) as a potent inhibitor of RSV, influenza B viruses and IAVs of human, avian, and swine origin. Biochemical i*n vitro* polymerase assays and viral RNA sequencing revealed that the ribonucleotide analog is incorporated into nascent viral RNAs in place of cytidine, increasing the frequency of viral mutagenesis. Viral passaging in cell culture in the presence of inhibitor did not induce robust resistance. Pharmacokinetic profiling demonstrated dose-dependent oral bioavailability of 36-56%, sustained levels of the active 5'-triphosphate anabolite in primary human airway cells and mouse lung tissue, and good tolerability after extended dosing at 800 mg/kg/day. The compound was orally efficacious against RSV and both seasonal and highly pathogenic avian IAV in mouse models, reducing lung virus loads and alleviating disease biomarkers. Oral dosing reduced IAV burden in a guinea pig transmission model and suppressed virus spread to uninfected contact animals through direct transmission. Based on its broad-spectrum efficacy and pharmacokinetic properties, NHC a promising candidate for future clinical development as a treatment option for influenza-like diseases.

42 **Introduction**

43 The clinical burden of respiratory viruses associated with influenza-like diseases is highest for the
44 elderly, the immunocompromised, and the very young. Patients above 65 years of age, for instance,
45 are most heavily affected by seasonal influenza, followed by infants (1). Although an inverse patient
46 age group distribution is seen for respiratory syncytial virus (RSV), a member of the *Pneumoviridae*
47 family, the substantial threat caused by severe RSV disease to the elderly is increasingly appreciated
48 (2) and case fatalities associated with both influenza virus and RSV infections disproportionally affect
49 older adults (3). Amplifying the need for next-generation antiviral therapeutics for improved
50 management of respiratory virus infections, the effectiveness of the current tri- or quadrivalent influenza
51 vaccine is limited to approximately 60% in adults and only 40% in the elderly even under the best
52 circumstances (4). However, substantially lower vaccine efficacy is seen for instance in the particularly
53 severe 2017/2018 influenza season (5). No active vaccination is currently available to protect against
54 RSV infection. Passive monoclonal antibody immunoprophylaxis can be administered to high-risk
55 patients, but an estimated $300,000 cost to prevent a single RSV hospitalization (6-11) is prohibitive to
56 broad application.

57 Since seasonal influenza and RSV outbreaks overlap in temperate regions, clinical symptoms are
58 often non-specific, and laboratory typing is often not routine outside of clinical centers and/or hampered
59 by cost constrains (1), an umbrella diagnosis of influenza-like disease with unclear nature of the
60 etiologic agent remains common. This ambiguous diagnosis compromises the efficacy of antiviral
61 agents with anticipated narrow therapeutic windows (12-14). We therefore propose that next-generation
62 therapeutics with a broad antiviral indication spectrum including, as a minimum, influenza viruses and
63 RSV will be required to improve the management of influenza-like disease.

64 Generating truly broad-spectrum inhibitors has been a long-coveted goal of antiviral drug
65 development. Discovery efforts have concentrated mainly on two areas: i) host-targeted antivirals that
66 are immunomodulatory or interfere with cellular factors required for successful virus replication; and ii)
67 direct-acting inhibitors targeting a druggable site or activity conserved across different viral families.

Therapeutic targeting of host factors recruited for virus replication has attracted renewed interest in the past decade due to the combined promise of expanding the antiviral indication range and reducing the frequency of viral escape from inhibition (15-18). Although host-directed candidates have largely met these expectations in experimental settings (15, 16), the approach has yet to deliver approved therapeutics with safety profiles acceptable for human use against viral diseases such as seasonal influenza and RSV disease (19). Direct-targeted antivirals typically display more promising initial toxicity profiles, but the quest for broad-spectrum inhibitory activity has fueled the rediscovery of many promiscuous, often covalently reactive scaffolds that are associated with unclear mechanisms of activity (20-23). Based on their demonstrated history of ultimate failure in development, many of these scaffolds are considered undesirable and were classified as frequently hitting pan-assay interfering (PAIN) substances (21, 24). As a notable exception, different ribonucleoside analogs have been identified that combine good clinical promise with a broadened indication spectrum, often showing remarkable preference for a range of viral over host cell polymerases.

While no nucleoside analog inhibitor is currently in clinical use against influenza viruses in the United States, the allosteric endonuclease blocker baloxavir marboxil (xofluza) was recently approved for sale in Japan. Furthermore, ribavirin is licensed for the treatment of RSV infection and T-705 (favipiravir) is conditionally approved for stockpiling in Japan in a situation when a pandemic is caused by oseltamivir-resistant influenza virus. However, toxicity liabilities and limited efficacy undermine the clinical use of ribavirin (25, 26) and the potential for teratogenicity (27) may compromise the use of T-705 for the treatment of influenza. The ribonucleoside analog ALS-8176 was found to be efficacious in a human RSV challenge study (28), providing important proof-of-concept for the treatment of influenza-like diseases with competitive polymerase inhibitors, but ALS-8176 did not inhibit influenza virus (29).

Towards the ultimate goal of identifying developable broad-spectrum medications against influenza-like disease, we have established and validated a replication-competent dual RSV and influenza A virus (IAV) reporter virus-based high throughput screening (HTS) assay that allows the simultaneous identification of IAV-specific, RSV-specific, and dually active, potentially broad-spectrum,

hit candidates (30). The first implementation of this protocol against a large open discovery library of small-molecule compounds has yielded promising target-specific inhibitors of RSV (31) and influenza virus (32), but broad-spectrum hits remained limited to undesirable scaffolds and clinically undevelopable compounds interfering with pyrimidine *de novo* synthesis (32-34). In this study, we applied the assay to a collection of ribonucleoside analogs. Having identified a cytidine analog with potent activity against both target viruses, we initiated mechanistic characterization of RSV and IAV RNA-dependent RNA polymerase (RdRp) inhibition, evaluated potency against a panel of laboratory adapted and clinical strains representing RSV, IAVs and influenza B viruses (IBVs) in established cell lines and primary human bronchial tracheal epithelial cells (HBTECs), determined oral pharmacokinetic profiles in the murine respiratory tract, assessed potency against RSV and both seasonal and highly pathogenic IAV subtypes in mouse models, and examined the effect of treatment on influenza virus spread in the guinea pig IAV transmission model. Collectively, these assays identify the compound as an orally efficacious broad-spectrum inhibitor of influenza-like disease caused by RSV or influenza virus infections.

108 **Results**

109 Having assembled an in-house library of 102 ribonucleoside analog candidates, we sampled the
110 set in three replicates using our validated dual-pathogen HTS protocol (30). This campaign yielded
111 three hit candidates that consistently blocked both viral targets in the primary assay, and in addition two
112 RSV-specific and one influenza virus-specific candidate (Fig. 1A).

113 **Indication spectrum of a dually-active HTS hit candidate**

114 Focusing on the dual-active compounds only, two candidates were excluded based on excessive
115 toxicity in dose-response potency and toxicity counterscreens (Fig. S1), while the remaining candidate
116 (dual #1, EIDD-1931 or N^4-hydroxycytidine (NHC) Fig. 1B) showed active concentrations in the
117 nanomolar to low-micromolar range and selectivity indices (SI = CC_{50}/EC_{50}) of ≥89 against a broad
118 panel of RSV, IAV, and IBV laboratory strains and isolates (Table 1). This group included clinical RSV
119 isolates cultured from nasal washes (Fig. 1C), IAVs of human, avian, and swine origin representing
120 both group 1 and 2 hemagglutinins (HAs), Fig. 1D and Table 1), highly pathogenic H5N1 and emerging
121 H7N9 avian IAVs (AIVs) (Fig. 1E), and IBVs representing both circulating lineages (35), Victoria and
122 Yamagata (Fig. 1F). A subset of avian influenza viruses was tested *in ovo* (Table 1), demonstrating
123 NHC potency in primary cells. Consistent with high initial SI values in cultured cells, embryo
124 development in the treated chicken eggs was visually unaffected by the compound (Fig. S2). Whereas
125 T-705 was inactive in primary HBTECs, antiviral activity of NHC against both RSV and influenza virus
126 was unchanged in these disease-relevant human primary cells compared to immortalized cell lines (Fig.
127 1G). Drug combination testing of NHC and the current standard of care (SOC) against IAV infection,
128 oseltamivir, in cultured cells identified an extended plateau area of medium-level antiviral synergy (HAS
129 model), while no significant increase in cytotoxicity was noted in the presence of drug combination (Fig.
130 S3). These data demonstrate activity of NHC against a panel of respiratory viruses associated with
131 influenza-like diseases. Combined with previously reported antiviral activity of NHC in cell culture
132 against some *Flaviviridae*, *Coronaviridae*, and *Togaviridae* family members (36-39), they establish
133 broad-spectrum activity of the compound against different positive- and negative-strand RNA virus

134 families and, in the case of IAV infection, spotlight potential for synergistic combination with the current
135 SOC.

136 **Mechanistic assessment of NHC**

137 Based on reversal of NHC-mediated inhibition of a Chikungunya virus replicon through an excess
138 of exogenous cytidine and uridine, the compound was thought to behave as a pyrimidine analog *in*
139 *cellula* (37). We first confirmed through time-of-addition variation studies that NHC blocks a post-entry
140 step in influenza virus and RSV replication cycles (Fig. 2A). Plasmid-based minigenome reporter
141 assays validated in both cases NHC interference with viral RdRp activity (Fig. 2B). However, an *in vitro*
142 activity assay using host cell polymerase α did not reveal inhibition of the cellular polymerase by the
143 active 5'-triphosphate form of the compound, NHC-TP (Fig. 2C). As previously observed for positive-
144 strand RNA-virus replicons, inhibition of RSV and influenza virus by NHC can be reversed through
145 addition of exogenous pyrimidines but not purines (Fig. 2D). To determine whether NHC-TP is
146 accepted by negative-strand RNA virus RdRps as substitute for CTP or acts as a chain-terminator, we
147 employed a biochemical assay of RSV polymerase activity that uses purified viral phosphoprotein (P)
148 and large protein (L) RSV polymerase components, NTP mix, and a synthetic oligonucleotide template,
149 resulting in a 23-mer product (40). Without CTP in the NTP mix, polymerization is stalled at the first
150 guanidine residue in the template, releasing 14-mer amplicons. Addition of NHC-TP partially restored
151 the generation of full-length 23-mer amplicons, demonstrating that the RSV RdRp complex accepts
152 NHC in place of cytidine and that the compound does not act as an obligatory chain-terminator (Fig.
153 2E). Rather, we noted a significantly increased frequency of C-to-U, G-to-A, and, in the case of RSV
154 only, A-to-G transition mutations in viral RNA after single-cycle infection of cells in the presence of 10
155 μM NHC, followed by subcloning of individual viral RNA-derived cDNA amplicons and Sanger
156 sequencing (Fig. 2 F). Relative mutation frequencies were increased approximately 7-10-fold (Table 2),
157 but no specific mutation hot-spots were detected in the fragment analyzed. This observation is
158 consistent with a postulated ability of NHC to base-pair as either cytosine or uracil (41), which may
159 drive the replicating viruses into error catastrophe (36, 42).

160 Previous attempts to induce robust resistance of two positive strand RNA viruses, Venezuelan
161 equine encephalitis virus and bovine viral diarrhea virus, from inhibition by NHC were unsuccessful (36,
162 43). To resistance profile negative-strand RNA virus-derived RdRps, we incubated RSV-A2 and IAV-
163 WSN in the presence of gradually increasing NHC concentrations for 10 consecutive passages.
164 However, no robust resistance (> 5-fold increase in EC_{50} concentrations) emerged, indicating a
165 universally high barrier against viral escape from NHC, independent of the target virus examined.

166 **Pharmacokinetics**

167 In preparation for *in vivo* testing, we determined anabolic, pharmacokinetic (PK), and
168 pharmacodynamic (PD) profiles and lung tissue distributions of the compound in primary HBTECs and
169 mice. LC/MS/MS analysis after exposure of HBTECs to 20 μM NHC demonstrated effective conversion
170 to active NHC-TP, represented by an approximately 4 nanomoles/10^6 cells concentration plateau over
171 the 24-hour time period examined. By contrast, steady-state levels of free prodrug and NHC-
172 5'monophosphate (NHC-MP) remained flat at a low ~2 pmoles/10^6 cells in this period (Fig. 3A).
173 Subsequent wash-out revealed high metabolic stability of NHC-TP in the HBTECs, resulting in a
174 calculated half-life exceeding 4 hours (Fig. 3B).

175 For species consistency with our mouse efficacy models of RSV and IAV infection, we determined
176 plasma PK of NHC and lung levels of both NHC and the active antiviral agent NHC-TP in mice.
177 Intraperitoneal (I.P.) and oral (p.o.) administration different dose levels ranging from 10 to 50 mg/kg
178 (I.P.) and 50 to 500 mg/kg (p.o.) resulted in dose-dependent increases in overall exposure (AUC) to the
179 prodrug (Fig. 3C) and peak plasma concentrations (C_{max}) after oral dosing exceeding 40 μM (Fig. 3D).
180 Exposure levels corresponded to a dose-dependent oral bioavailability of 36 to 56% (Table 3). Dose-
181 dependency of overall prodrug exposure extended to respiratory tissue (Fig. 3E), but peak NHC-TP
182 concentrations in lung saturated above oral dose levels of approximately 150 mg/kg (Fig. 3F). While
183 this C_{max} plateau suggests an anabolism bottleneck of NHC in mouse respiratory tissue at higher
184 prodrug levels, lung tissue distribution assessment revealed sustained concentrations of active NHC-
185 TP of approximately 10 nanomoles/g lung tissue for over 8 hours after administration at the 150 and

500 mg/kg levels. These results highlight the strong potential of NHC for clinical use against influenza-like diseases.

In vivo efficacy testing against major causes of influenza-like diseases

Based on the PK/PD profiles, we selected as starting point for all experiments oral doses of 100 mg/kg (below NHC-TP lung tissue plateau level) and 400 mg/kg (comfortably within NHC-TP tissue saturation range), and a twice daily (b.i.d.) dosing regimen for *in vivo* efficacy testing against RSV and IAV in mice. For testing against RSV, BALB/cJ mice were infected intranasally (i.n.) with 10^5 pfu each of recombinant RSV A2-L19F, which is based on the A2 strain but contains an F protein derived from the RSV isolate line 19 that increases pathogenicity in the mouse model and better reproduces key features of human RSV disease such as high lung virus load, extensive mucus production, and pronounced respiratory distress (44). Treatment was initiated two hours prior to infection and continued until lung virus titers were determined five days post-infection. At both dose levels, RSV loads were significantly reduced by more than one order of magnitude compared to vehicle-treated animals (Fig. 4A). However, we did not detect an appreciable difference in progeny titers between the dose groups, presumably reflecting that even at the lower dose used NHC-TP concentration in lung tissue approaches saturation levels. Lung histopathology and PAS staining demonstrated complete suppression of excessive mucin production in the 400 mg/kg group and a partial reduction in animals dosed with 100 mg/kg (Fig. S4). Exploratory dosing at 30 and 50 mg/kg failed to significantly lower lung virus load (Fig. S5), but oral doses as low as 30 mg/kg were sufficient to completely ameliorate the severe respiratory distress experienced by vehicle-treated animals (Fig. 4B). These results demonstrate effective inhibition of RSV replication by NHC *in vivo* at higher dose concentrations. The data furthermore suggest that even minimal pharmaceutical interference with RSV replication can translate into major changes in RSV disease markers in the mouse model.

To test NHC efficacy against seasonal influenza viruses, we infected BALB/cJ mice i.n. with 10^3 pfu of mouse-adapted A/Puerto Rico/8/34 (H1N1) (PR8) and assessed lung viral load six days post-infection as the primary efficacy milestone. In addition, virus-induced hypothermia and selected pro-

inflammatory cytokines were monitored. Based on the experience with anti-RSV efficacy, we focused on the 100 and 400 mg/kg dose levels only for these experiments. After prophylactic dosing as before, we again observed significant reductions in lung virus load in NHC versus vehicle-treated animals (Fig. 4C). All infected animals experienced virus-induced hypothermia, but symptoms were significantly alleviated in mice treated with high-dose NHC (Fig. S6). To put the antiviral impact of NHC in perspective to SOC, we orally administered NHC (400 mg/kg dose level only in this experiment) or oseltamivir to PR8 infected mice and determined lung virus load profiles for each treatment group (Fig. 4D). Consistent with previous observations (45), oseltamivir delayed viral replication in the first 2 days after infection, but peak lung titers in the oseltamivir group were not significantly different from those in vehicle-treated animals. In contrast, treatment with NHC caused a significant and sustained reduction in virus load. RT-qPCR-based quantitation of virus-triggered induction of selected pro-inflammatory cytokines, IFN-γ and IL-6, revealed a statistically significant decrease in mean induction levels in the 400 mg/kg group (Fig. 4E).

Since PR8 reaches plateau lung titers within 24 hours after infection (Fig. 4D), the time window provided by the mouse model to assess post-exposure efficacy of NHC is narrow. To gain first insight into the effect of delayed dosing onset, we initiated treatment at six hours post-infection, again administering the compounds at the 400 mg/kg dose level only and continuing with a b.i.d. regimen. Lung virus loads were determined three and six days post-infection, and at both time points showed a significant reduction compared to vehicle-treated control animals (Fig. 4F). In keeping with the results obtained after prophylactic dosing, virus-induced hypothermia was significantly reduced in the post-exposure NHC-treated animals also (Fig. S6), establishing comparable benefit of NHC on management of influenza virus infection independent of whether treatment followed a prophylactic or post-exposure regimen.

Efficacy against highly-pathogenic avian influenza virus and effect on IAV transmission

Having obtained proof-of-concept for oral NHC efficacy against PR8 in mice, we employed an HPAIV/mouse model to examine the potential of the compound to strengthen preparedness against

238 highly pathogenic IAVs that constitute a high pandemic threat. Mice were infected i.n. with 6 pfu of
239 A/Vietnam/1203/2004 (H5N1) (A/Vietnam), treatment initiated prophylactically at the 400 mg/kg dose
240 level only, and continued as before. Due to pronounced neuropathogenicity of A/Vietnam in the model
241 (46), both lung and CNS viral loads were determined at day six post-infection in comparison with
242 vehicle and SOC-treated animals (Fig. 4G). Lung virus titers were again significantly reduced in drug-
243 treated animals as compared to the vehicle-only group, and virus was undetectable in the CNS in four
244 out of five animals that had received NHC. This inhibitory effect on A/Vietnam lung virus load was
245 equivalent to that observed in oseltamivir-treated animals, but NHC more efficiently prevented HPAIV
246 dissemination to the CNS since three of the five animals in the oseltamivir treatment group presented
247 with detectable virus in brain tissue.

248 Since influenza virus does not transmit efficiently in mice (47), we employed the well-established
249 guinea pig IAV transmission model (48) to evaluate the effect of NHC on virus spread. Similar to
250 uncomplicated human influenza, virus replication in guinea pigs is limited predominantly to the upper
251 respiratory tract. Source animals were infected i.n. with 10^4 pfu of A/Netherlands/602/2009 pH1N1
252 (NL/09) virus and co-housed with uninfected contact guinea pigs starting 24 hours post-infection.
253 Treatment of the source group was initiated prophylactically at the 100 and 400 mg/kg dose levels and
254 continued b.i.d. as before. Source animals showed a significant, dose-dependent reduction in shedding
255 titers determined from nasal lavages that exceeded two orders of magnitude (Fig. 4H). Vehicle-treated
256 animals furthermore efficiently passed the virus to contact guinea pigs. Transmitted virus was first
257 detected at day four post-infection and titers peaked at approximately 10^6 pfu/ml of nasal wash on day
258 six after initiation of the study. By contrast, low-dose NHC treatment of source guinea pigs delayed
259 transmission by approximately one day, and titers remained below 10^4 pfu/ml of nasal wash throughout
260 the study (Fig. 4I). We noted an even more pronounced inhibitory effect on virus spread when source
261 animals were treated at the 400 mg/kg dose level. Weak transmission was detected in this group only
262 at day eight, and remained limited to two of the four contacts. The other contact animals remained

263 virus-free for the duration of the study. These studies demonstrate oral efficacy of NHC against major

264 pathogens associated with influenza-like illnesses in different animal models.

265 **Discussion**

266 Influenza-like illnesses show disproportionally high case fatalities in older adults (1-3). To
267 effectively address this problem, a next-generation therapeutic must be developed for this patient
268 population frequently suffering from seasonal influenza virus or RSV infection and presenting with
269 influenza-like symptoms. In addition to a reduction in viral load that is sufficient to prevent disease
270 progression to severe small airway infection and alleviate acute respiratory distress, a drug candidate
271 suitable for this patient group should best be orally available to ensure reasonable patient compliance.

272 Through a dual-pathogen (31, 32) HTS campaign that affords the simultaneous identification of
273 RSV and IAV inhibitors, we identified NHC, a pyrimidine ribonucleoside analog, as a hit candidate that
274 integrates promising potency with a broadened indication spectrum. NHC was previously associated
275 with antiviral activity against positive-strand RNA viruses (36-39), but PK/PD profiles have not been
276 determined and *in vivo* efficacy is untested.

277 The broad overall indication spectrum of NHC is reminiscent of that described for T-705 (favipiravir)
278 and ribavirin, two compounds that act after phosphoribosylation (T-705) and phosphorylation as purine
279 analogs, respectively, and are believed to interfere with RNA virus replication through pairing with either
280 cytidine or uridine (49, 50), resulting in high mutation frequencies and ultimately error catastrophe (42).
281 While T-705 is conditionally approved in Japan and considered for licensing in the United States, we
282 found the drug to be compromised by poor antiviral activity in primary human respiratory cells. In
283 contrast, NHC returned a consistent efficacy profile in immortalized cell lines and in disease-relevant
284 primary HBTECs, consistent with efficient conversion to active NHC-TP and high metabolic stability of
285 the 5'-triphosphate also in primary human airway cells.

286 Early studies suggested that NHC-TP can substitute for uridine or cytidine in RNA polymerase
287 reactions (51, 52). Three lines of experimental evidence support our hypothesis that the anti-influenza
288 virus and anti-RSV activity of NHC is predominantly the result of viral error catastrophe: i) an excess of
289 exogenous cytidine or uridine but not purines reverses compound-mediated inhibition, indicating that
290 NHC is recognized as a pyrimidine analog by the influenza virus and RSV RdRp complexes; ii) NHC-

291 TP can functionally substitute for CTP in a biochemical RSV polymerase assay using purified RdRp
292 complexes; and iii) growth of IAV-WSN and RSV-A2-L19F in the presence of sub-sterilizing NHC
293 concentrations resulted in an increased frequency of C-to-U, G-to-A, and A-to-G transition mutations.
294 The cell-based competition assays indicate that substrate-recognition of NHC-TP by RSV and IAV
295 polymerase is comparable to that of CTP, since at least equimolar concentrations of exogenous
296 cytidine were required to reverse NHC-mediated inhibition despite the micromolar levels of endogenous
297 ribonucleosides naturally present in the cells (53). Previous mutagenesis studies with both positive and
298 negative sense RNA viruses have shown that viral tolerance for an increase in mutation frequency is
299 limited (50, 54-56). For instance, an average of three random mutations per viral genome is sufficient
300 for an 80%-reduction in poliovirus specific infectivity (42). In our biochemical assays, however, NHC-TP
301 only partially restored RSV polymerase activity in the absence of CTP. This finding suggests that
302 incorporation of the compound may also reduce polymerase processivity and/or increase the likelihood
303 of chain termination. Of note, T-705 was also suggested to directly block influenza virus RdRp (57), and
304 a number of alternative antiviral effects were suggested for ribavirin including lowering of cellular GTP
305 levels, immunomodulation, blockage of RNA capping, and direct viral polymerase inhibition (58).
306 Conceivably, antiviral activity of NHC may arise from a combination of lethal mutagenesis and
307 kinetically impaired or abortive polymerization.
308 Previous work predicted a mutagenic effect of NHC based on restored growth of cytidine auxotroph
309 *S. typhimurium* JL1045 after exposure to the compound (59). However, this conclusion is flawed, since
310 NHC can be converted directly to cytidine by the mitochondrial amidoxime-reducing component
311 (mARC) (60), thus the drug itself and not compound-induced reversion mutants serves as pyrimidine
312 source for JL 1045. Consistent with this view, DNA repair mechanisms are not activated by NHC (61).
313 The anticipated treatment time of influenza and RSV disease is furthermore short – the recommended
314 course of oseltamivir, for instance, is 5-7 days (14) – and prolonged exposure to NHC was well
315 tolerated by both mice and guinea pigs.

316 Consistent across both positive- and negative-strand viral targets pursued, viral escape from
317 inhibition by NHC remains inefficient and extended passaging under conditions that we have
318 successfully optimized in previous studies for induction of resistance to allosteric antivirals (32, 62, 63)
319 failed to yield appreciably higher tolerance to NHC. A recent study aimed at inducing escape of
320 Venezuelan equine encephalitis virus (VEEV), a *Togaviridae* family member, from NHC inhibition found
321 that a combination of three distinct mutations in VEEV RdRp was required for partial escape (36).
322 However, subsequent viral passaging in the absence of compound resulted in rapid loss of resistance.
323 The appearance of preexisting resistance to available antivirals in circulating influenza viruses is a
324 major concern, having compromised the M2 ion channel blocker class (64) and affecting, increasingly,
325 the neuraminidase inhibitors (65-69). Although we have not yet determined *in vivo* resistance profiles of
326 the compound, the available data in aggregate suggest that a fitness penalty may prevent the rapid
327 accumulation of preexisting anti-NHC resistance mutations.
328 Based on PK profiles in mice indicating sustained high lung tissue concentrations of the antivirally
329 active NHC-TP anabolite, we chose the mouse models of RSV and IAV infection for small-animal
330 efficacy testing. While supporting productive infections, tissue tropism differs from human disease in
331 both models since virus replication occurs predominately in the small airways rather than the upper
332 respiratory tract (70-73). In the case of the IAV model, mice furthermore develop hypothermia rather
333 than fever (74) and do not cough or sneeze (47). In keeping with our overall therapeutic premise that
334 reducing progeny viral load will be paramount in preventing viral spread to the small airways and
335 severe lower respiratory tract infection in humans, we consider lung viral burden to represent the most
336 relevant readout to assess treatment efficacy in these models, although additional disease biomarkers
337 were monitored in parallel. The observed significant lung virus load reductions were consistent with
338 efficient NHC uptake and anabolism in primary cells, the antiviral activity of the compound in native cell
339 cultures and *in ovo*, and the sustained lung tissue concentrations of NHC-TP in mice. Virus titer
340 reductions were equivalent to, or exceeded those, reported for SOCs ribavirin (75) and oseltamivir (45)
341 in the mouse model.

342 Clinical studies and animal models have implicated a number of pro-inflammatory mediators in
343 playing a significant role in coordinating the innate immune response to influenza virus infection (76-
344 78). IL-6 in particular was identified as a promising biomarker for disease severity in the PR8 BALB/cJ
345 model based on correlation of IL-6 levels with viral titers (45, 79). Consistent with viral load reductions
346 in NHC treated animals, we found that relative IL-6 expression levels were significantly reduced in the
347 high-dose NHC treatment group, underscoring therapeutic benefit of the compound against influenza.
348 No robust small-animal RSV transmission model is available, but guinea pigs support efficient IAV
349 transmission. Although lacking overt signs of disease, guinea pigs are highly susceptible to infection by
350 human influenza viruses. Virus replication to high titers in the guinea pig upper respiratory tract,
351 resembling a hallmark of uncomplicated influenza in humans, furthermore generates a basis for
352 efficient direct and aerosol transmission (48). In addition to substantially lower viral loads in treated
353 source animals that corroborated the results of the mouse efficacy studies, reduced IAV transmission
354 success under NHC treatment generates high promise that human therapy with NHC may accelerate
355 silencing of virus outbreaks in addition to improving management of influenza-like disease.
356 NHC emerges from this first *in vivo* efficacy assessment study as an orally active ribonucleoside
357 analog with potent activity against influenza viruses and RSV. The compound was highly bioavailable,
358 efficiently converted to the active NHC-TP form in disease-relevant respiratory tissues, well tolerated,
359 and did not induce rapid viral escape from inhibition. NHC was effective against seasonal and highly
360 pathogenic avian IAV strains, IBV strains, and RSV isolates in cell culture. Treatment alleviated clinical
361 markers of RSV and influenza virus disease in the mouse model and effectively reduced influenza virus
362 host-to-host spread in a guinea pig transmission model. We consider NHC or a prodrug analog thereof
363 to be worthwhile of further consideration as a promising candidate for the treatment of influenza-like
364 diseases.

365 **Materials and Methods**

366 **Cell lines and transfections**

367 Human embryotic kidney cells (293T; ATCC CRL-3216), Madin-Darby canine kidney cells (MDCK;
368 ATCC CCL-34), HEp-2 cells (ATCC CCL-23) and baby hamster kidney cells (BHK-21; ATCC CCL-10)
369 stably expressing T7 polymerase (BSR T7/5) were maintained at 37°C and 5% CO_2 in Dulbecco's
370 modified Eagle's medium (DMEM) supplemented with 7.5% fetal bovine serum (FBS). HEp-2 cells are
371 listed in ICLAC database Version 8.0 of commonly misidentified cell lines, but their use is justified as
372 these cells are accepted and widely used for studies involving respiratory syncytial virus (RSV).
373 GeneJuice transfection reagent (Invitrogen) was used for all transfection reactions. Normal primary
374 Human Bronchial Tracheal Epithelial Cells (HBTECs purchased from LifeLine Cell Technology (Cat.
375 No. LM-0050), passage number 1-3) were grown in BronchiaLife Cell Culture Medium (LifeLine Cell
376 Technology). Immortalized cell lines used in this study are routinely checked for microbial
377 contamination (in approximately 6-month interval). HBTECs were tested for microbial contamination on
378 July 25, 2017 by LifeLine Cell Technology. These cells were grown for 2 weeks for this study after that
379 the testing.

380 **Viruses**

381 Influenza viruses A/WSN/33(WSN) (H1N1), WSN-nanoLuc, A/California/7/2009 (H1N1),
382 A/Georgia/M5081/2012 (H1N1), A/Netherlands/602/2009 (H1N1), A/Panama/2007/99 (H3N2),
383 A/Wisconsin/67/2005 (H3N2), influenza A/Aichi/2/68 (H3N2), A/swine/Ohio/sw10-132/2010 (H3N2),
384 B/Yamagata/16/88, and B/Brisbane/60/08 were propagated in MDCK cells for 2 days at 37°C. Influenza
385 viruses A/duck/Alberta/35/76 (H1N1), A/swine/Spain/53207/2004, and A/Chicken/Potsdam/178-4/83
386 (H2N2) were propagated in 10-day-old embryonated chicken eggs for 2 days at 37°C. Influenza viruses
387 A/Vietnam/1203/2004 (H5N1) and A/Anhui/1/2013 (H7N9) were propagated in 9-day-old embryonated
388 chicken eggs at 37°C for 24 hours. All experiments using live, highly pathogenic H7N9 avian influenza
389 viruses were reviewed and approved by the institutional biosafety program at the University of Georgia,
390 were conducted in biosafety level 3 enhanced containment, and followed guidelines for use of Select

391 Agents approved by the CDC. Viruses were titrated by standard plaque assays, hemagglutination
392 assays (80), $TCID_{50}$ assays, or $TCID_{50}$-hemagglutination ($TCID_{50}$-HA) assays in MDCK cells. For
393 $TCID_{50}$-HA assays, 10-fold serial dilutions of virus samples in eight replicates each were propagated for
394 48 hours on MDCK cells in a 96-well plate format, followed by transfer of culture supernatants to
395 suspensions of chicken red blood cells and scoring of individual wells based on hemagglutination
396 activity. Clinical RSV isolates were collected from patient nasal washes in 2010, cultured on primary
397 rhesus monkey kidney (RhMK) cells, and amplified once on HEp-2 cells prior to use in this study.
398 Recombinant RSV and RSV isolates were grown in HEp-2 cells and titrated by plaque or
399 immunoplaque assay in HEp-2 cells.

400 **Purification of recombinant reporter virus stocks**

401 Progeny virions were collected from cell culture supernatants (IAV) or released from infected cells
402 through one freeze-thaw cycle (RSV) and subjected to a clearance centrifugation (4,000 rpm for 20 min
403 at 4°C). Virions were diluted in DMEM, purified through a 20%-60% one-step sucrose gradient in TNE
404 buffer (1 mM Tris [pH 7.2], 100 mM NaCl, 10 mM EDTA; 30,000 rpm for 120 min at 4°C), and harvested
405 from the gradient intersection. Purified virus stocks were stored in aliquots at −80°C.

406 **Automated drug screening**

407 MDCK cells were injected into barcoded white-walled/clear-bottomed 384-well plates using a
408 MultiFlo automated dispenser (BioTek) equipped with dual 10-µl peristaltic pump manifolds and
409 incubated for 5 hours at 37°C and 5% CO_2. Compounds were added to a final concentration of 5 µM
410 (20 nl/well) by using a high-density pin tool (V&P Scientific), followed by coinfection with recRSVA2-
411 L19F-fireSMASh (multiplicity of infection [MOI] = 0.1) and recIAV-nanoLuc (MOI = 0.02) at 10 µl/well by
412 use of a MultiFlo dispenser unit, and incubation for 48 h at 37°C and 5% CO_2. The final vehicle (DMSO)
413 concentration was 0.05%. The reporter gene activity was recorded 48 hours post-infection with H1
414 synergy multimode plate reader (BioTek), and compounds showing ≥80% inhibition of both RSV and
415 IAV pursued as hit candidates. The MScreen software package was used for library management and
416 campaign analysis.

417 **Dose-response antiviral activity and cytotoxicity testing in cultured cells**

418 For automated dose-response testing, three-fold serial dilutions were prepared in 96-well plates in
419 three replicates each using a Nimbus liquid handler (Hamilton). Target cells as specified were seeded
420 in white-wall clear-bottom 96-well plates (8×10^3 cells/well) and the serial dilutions transferred using the
421 liquid handler, followed by infection with IAV-WSN-nanoLuc (MOI 0.02) or RSV-A2-L19F-fireSMASh
422 (MOI 0.1). Reporter signals were recorded with the H1 synergy plate reader specified above. To
423 determine cell viability, PrestoBlue substrate (5 µl/well (Life Technologies)) was added after 48 h
424 incubation of compound-exposed uninfected cells at 37°C and top-read fluorescence (excitation at 560
425 nm, emission at 590 nm, instrument gain of 85) recorded after incubation for 45 min at 37°C using the
426 H1 synergy plate reader. Raw data of all automated dose-response assays were analyzed according to
427 the formula % inhibition = $(X_{Sample}-X_{Min})/(X_{Max}-X_{Min})\times100$ with X_{Min} representing the average of four
428 positive (1 mg/ml cycloheximide) and X_{Max} the average of four negative (DMSO) control wells included
429 on each plate. Four-parameter variable slope regression modeling was applied to determine 50% active
430 (EC_{50}) and toxic (CC_{50}) concentrations, using the non-linear regression function in the Prism
431 (GraphPad) software package. For manual dose-testing of non-reporter viruses, target cells were
432 seeded in 12-well plates (1.5×10^5 cells/well) and at approximately 90% confluency infected with the test
433 virus in the presence of serial compound dilutions. Progeny virus titers were determined 36 to 48 hours
434 post-infection depending on the virus strain analyzed, and viral titers determined as described above.

435 **Human DNA polymerase inhibition assay**

436 Inhibition of human DNA polymerase α was assayed in a 96-well format containing reaction buffer
437 (50 mM Tris-HCl (pH 8.7), 10 mM $MgCl_2$, 0.4 mg/ml BSA, 1 mM DTT, 15% glycerol, 0.05 mM dCTP,
438 0.05 mM dTTP, 0.05 mM dATP, 10 µCi [^{32}P]-α-dGTP (800 Ci/mmol)), 20 µg activated calf thymus DNA,
439 and NHC-TP in a range of different concentrations. Alphidicolin served as polymerase inhibitor
440 reference. Reactions were carried out for 30 minutes at 37°C, followed by transfer to filter plates,
441 precipitation with 10% trichloroacetic acid and repeated washing with 5% trichloroacetic acid and 95%

ethanol. Incorporation of [α-^{32}P] GTP was measured after filter drying using a Microbeta scintillation counter.

Efficacy against IAV *in ovo*

Serum pathogen-free (SPF) freshly fertilized chicken eggs were purchased from Hy-Line and incubated at 37°C, 55-60% humidity for 10 to 11 days. Eggs were candled, disinfected with 70% ethanol, and NHC in sterile PBS was administered to a final concentration of approximately 10 µM directly into the allantoic fluid 2 hours prior to infection using a 22-gauge needle. The average volume of the allantoic fluid was considered to be 50 ml. Eggs were sealed and incubated for 2 hours, followed by infection with 10 HA units of A/Swine/Spain/53207/2004 (H1N1). After 48-hours incubation, eggs were cooled to 4°C, virus harvested from the allantoic fluid and titrated using standard hemagglutination (HA) assays and turkey red blood cells.

Replicon reporter assays

Reporter activities were determined in the presence of three-fold serial dilutions of NHC starting from 20 µM for RSV and 100 µM for IAV; treatment was initiated immediately post-transfection. Luciferase activities in cell lysates were measured in a Synergy H1 microplate reader (BioTek) in top-count mode using Dual-Glo Luciferase Assay System (Promega). Inhibitory concentrations were calculated through four-parameter variable slope regression modeling.

Time-of-addition variation studies

HEp-2 cells were infected with 0.1 MOI RSV-A2-fireSMASh and MDCK cells were infected with 0.05 MOI of IAV WSN-nanoLuc. At the specified time points relative to infection, NHC, GRP-71271, AL-8176, or CL-309623 were added to the culture media to a final concentration of 10 µM. T-705 was added to a final concentration of 50 µM and volume equivalents of DMSO served as vehicle controls. Reporter gene expression was measured 24 (IAV WSN-nanoLuc) or 48 (RSV-A2-fireSMASh) hours post-infection, and the obtained values expressed relative to the vehicle-treated samples.

Nucleotide competition experiments

467 HEp-2 cells were infected with 0.1 MOI RSV-A2-fireSMASh and MDCK cells were infected with
468 0.05 MOI of IAV WSN-nanoLuc. At the time of infection, NHC was added to a final concentration of 10
469 µM NHC alone, or in combination with 0.1 to 300 µM exogenous nucleosides (Sigma-Aldrich). Volume
470 equivalents of DMSO served as vehicle control. Reporter gene expression was quantified 24 (IAV-
471 WSN-nanoLuc) or 48 (RSV-A2-fireSMASh) hours post-infection. Values are expressed relative to the
472 vehicle-treated samples.

473 ***In vitro* RSV polymerase assay**

474 RSV large polymerase subunit (L) and phosphoprotein (P) complexes were expressed from a
475 baculovirus vector and purified by affinity chromatography: L-P complexes were eluted from the Ni-NTA
476 column with 250 mM imidazole in 50 mM NaH_2PO_4, pH 7.5, 150 mM NaCl and 0.5% NP-40 followed by
477 dialysis against 150 mM NaCl, 20 mM Tris-HCl, pH 7.4, 1 mM DTT and 10% glycerol. L-P hetero-
478 oligomers were mixed in a Mg^{2+} buffer with 25-mer RNA oligonucleotide template containing essential
479 RSV promoter sequences and rNTPs including 0.07 µM [α-^{32}P]-UTP tracer, but lacking CTP. NHC,
480 NHC-TP, or CTP were added as specified. Predominant initiation at the +3 position results in up to 23-
481 mer radiolabeled amplicons, which were subjected to denaturing gel electrophoresis, followed by
482 autoradiography.

483 **Assessment of mutation frequencies in viral RNA**

484 HEp-2 cells were infected with 0.1 MOI RSV-A2-mKate and MDCK cells were infected with 0.05
485 MOI of IAV-WSN, followed by growth in the presence of 10 µM NHC for 24 hours; volume equivalents
486 of DMSO were used as vehicle control. Total RNA was extracted using the ZR Viral RNA Kit (Zymo
487 Research), cDNA of viral message synthesized with SuperScript III reverse transcriptase (Thermo
488 Scientific) and oligo dT primers. The PB1 segment of IAV-WSN or an approximately 1500 nucleotide
489 fragment of the RSV-A2-mKate L ORF were amplified by PCR and subcloned into pUC19 vector. For
490 each virus and treatment condition, at least 10 distinct subclones (equaling in aggregate at least
491 approximately 7500 nucleotides each) were Sanger sequenced using universal M13 primers. Data
492 were analyzed with Sequencer package and mutation frequencies expressed per 5000 nucleotides for

IAV-WSN and per 10,000 nucleotides for RSV-A2, respectively. Fisher's exact test was used for statistical analyses.

Virus adaptation in cell culture

Both dose-escalation and fixed dose adaptation strategies were applied. For dose escalation, MDCK cells were infected with 0.01 MOI of IAV-WSN and HEp-2 cells were infected with 0.1 MOI of RSV-A2-mKate. The viruses were passaged in the presence of increasing concentration of NHC, starting at 250 nM. Dose concentrations were doubled at virus passage up to a final concentration of 10 µM. Six independent passage lines each per target virus were advanced simultaneously for a total of ten passages, each entailing virus harvest from infected cells, dilution, and reinfection of fresh cell populations in the presence of compound or vehicle. Virus titers declined significantly towards the end of the series and no resistant variants emerged. For fixed dose adaptation, MDCK cells were infected with 0.01 MOI of IAV-WSN or B/Brisbane/60/08, HEp-2 cells infected with 0.1 MOI of RSV-A2-mKate. The viruses were passaged in the presence of EC_{99} concentration equivalents of NHC for the respective target virus, as before for a total of ten passages. Progeny virus titers again declined towards the end of the cycle and no drug-resistant virus population could be cultivated.

Anabolism and turnover in cultured cells

To screen for cellular uptake and anabolism of NHC to NHC-TP, HBTECs were grown in the presence of 20 µM NHC for 0, 1, 2, 3, 4, 6, 16 and 24 hours. Cells were washed with PBS, lysed with 70% methanol, and clarified samples stored at -20°C until analysis. To determine stability of NHC-TP and other anabolites, the HBTEC cells were grown in the presence of 20 µM NHC for 24 hours, media changed to drug-free BronchiaLife Cell Culture Medium, and cells incubated for an additional 0, 0.5, 1, 2, 3 and 6 hours. Metabolites were extracted with 70% methanol as before and samples kept at -20°C until analysis. NHC anabolites were quantitated using internal standards-based LC-MS/MS on an Agilent 1200 system (Agilent Technologies) equipped with a SeQuant ZIC-pHILIC column (The Nest group) column. Mass spectrometry analysis was performed on a QTrap 5500 Mass Spectrometer (AB

518 Sciex) using Negative Mode Electrospray Ionization (ESI) in Multiple Reaction Monitoring (MRM) Mode.
519 Data analysis was performed using Analyst Software (AB Sciex).

520 **PK and PD studies in mice**

521 Female CD-1 mice (6-8 weeks of age) distributed randomly to groups were dosed p.o. with NHC in
522 240 mM citrate buffer, followed by blood and lung tissue sampling. Plasma was purified from
523 heparinized blood, tissue samples were snap frozen prior to 70% acetonitrile extraction. Drug
524 concentrations were determined using $^{13}C_5$-labeled internal standards for NHC and NHC-TP. Mass
525 spectrometry was performed as detailed above. For calibration, standard curves were prepared in blank
526 plasma (concentrations range 25 to 30,000 ng/ml) and blank tissue lysate (concentration range 1.49 to
527 1,490 ng/ml). Quality-control samples of 30, 500 and 900 ng/ml in blank plasma were analyzed at the
528 beginning of each sample set. Calibration in each matrix showed linearity with an R^2 values >0.99.

529 **Mouse model for RSV infection**

530 Female BALB/cJ mice (5-6 weeks of age) were obtained from the Jack Laboratory or Envigo,
531 rested for one week, assigned to groups randomly anesthetized by intraperitoneal injection of a
532 ketamine-xylazine solution and infected i.n. with 1×10^5 pfu of recRSV A2-L19F. NHC was administered
533 orally in 240 mM citrate buffer or vehicle volume equivalent 2 hours pre-infection and dosing continued
534 b.i.d. for up to 8 days. For virus load titration, lungs were extracted, homogenized, homogenates
535 serially diluted, transferred to HEp-2 cells, and cells overlaid one hour post-infection with minimum
536 essential medium (MEM) containing 10% FBS, penicillin G, streptomycin sulfate, amphotericin B
537 solution, and 0.75% methylcellulose. Six days post-infection, cells were fixed with methanol and
538 plaques visualized by immunodetection. To quantify mucin expression, mice were euthanized eight
539 days post-infection, heart-lung tissue harvested, and fixed in 10% formalin. Lung tissue sections
540 embedded in paraffin blocks were stained with periodic acid-Schiff (PAS) stain and slides digitally
541 scanned using a Zeiss Mirax Midi microscope (Carl Zeiss Microimaging). To determine respiratory
542 distress noninvasively, a rodent pulse oximeter (MouseOx; Starr Life Sciences Corp., Oakmont, PA)
543 was applied to the mouse's thigh and arterial O_2 saturation, heart rate, pulse rate, pulse distension, and

544 breath distension measured every 0.1 seconds for a 1-5 minute overall period. Mean breath distension
545 for each treatment group was calculated based on mean values of all measurements for each animal in
546 which all target parameters were present.

547 **Mouse model for IAV infection**

548 Female BALB/cJ mice (6-8 weeks of age) were received from Envigo and housed ABSL-2 (for
549 infection with IAV-PR8) or ABSL-3 (for infection with HPAIV) facilities in HEPA-filtered microisolator
550 caging. Mice were rested for one week, weighed, assigned to groups randomly, and infected with 10^3
551 pfu of IAV-PR8 or 6 pfu of A/Vietnam/1203/04 (H5N1) as specified in PBS. Treatment was initiated 2
552 hours pre-infection (prophylactic dosing) or 6 hours post-infection (therapeutic dosing) and continued
553 for up to 6 days b.i.d. Compounds or vehicle volume equivalents were administered orally in 240 mM
554 citrate buffer formulation. Animal clinical signs were tracked daily, and animals euthanized at the
555 indicated time points or when humane endpoints were reached. Lung and, where indicated, brain tissue
556 were removed, homogenized, clarified by centrifugation, and aliquots frozen at -80°C as outlined above
557 until virus titration.

558 **Select cytokine mRNA induction in mouse lung tissue**

559 Relative IFN-γ and IL-6 induction levels present in mouse lung tissue were determined by semi-
560 quantitative real-time PCR analysis. Total RNA was extracted from lung tissue three days post-infection
561 of animals with IAV-PR8 or mock-infected (representing day 0). Infected animals were treated orally
562 with NHC or vehicle (citrate buffer) volume equivalents. RNA was reverse-transcribed with SuperScript
563 III reverse transcriptase and the resulting cDNAs subjected to real-time PCR using the Fast SYBR
564 Green Master Mix (Applied Biosystems). Glyceraldehyde-3-phosphate dehydrogenase (GAPDH)
565 mRNA served as an internal control, and mRNA induction levels were normalized to the average of the
566 values obtained determined for mock-infected animals. Each biological repeat was determined in
567 duplicate and relative changes in transcription levels calculated according to fold change = $2^{-\Delta\Delta CT}$.

568 **Guinea pig IAV infection and transmission model**

Female Hartley strain guinea pigs weighing 250 to 300 g were obtained from Charles River Laboratories. The animals were assigned to groups randomly, and prior to intranasal inoculation, nasal lavage, or CO_2 euthanasia, the guinea pigs were sedated with a mixture of ketamine and xylazine (30 mg/kg of body weight and 4 mg/kg, respectively). Inoculation and nasal lavage were performed with phosphate-buffered saline (PBS) as the diluent/collection fluid in each case. Oral treatment of infected donor animals with NHC or vehicle (240 mM citrate buffer with Ora-Sweet (Paddock Laboratories)) was initiated two 2 hours pre-infection and continued b.i.d. until the end of day 3 post-infection. Following inoculation and recovery from sedation, donor guinea pigs were housed in Caron 6040 environmental chambers (fitted with the optional dryer package) set to 10°C and 20% relative humidity. At 24 hours post-inoculation of the donor animals, exposed guinea pigs were introduced into the donor animal cages. Conditions of 10°C and 20% relative humidity were maintained throughout the exposure period, which ended on day 8 post-inoculation. Virus shedding titers in nasal lavages of source and contact animals were determined through plaque assays.

Statistical analysis

To assess experimental variation and the statistical significance of differences between sample means, one-way or two-way analysis of variance (ANOVA) were carried out in combination with Tukey's, Dunnett's, or Sidak's post hoc test as specified in figure legends, using the Prism (GraphPad) software package. Fisher's exact test was used for statistical analyses of mutation frequencies. Results for individual biological replicates are shown for all *in vivo* efficacy experiments. When appropriate, experimental uncertainties are identified by error bars, representing standard deviations (SD).

IACUC approval statement

All animal work was performed in compliance with the *Guide for the Care and Use of Laboratory Animals* of the National Institutes of Health. Mouse work at Georgia State University was approved by the GSU Institutional Animal Use and Care Committee (IACUC) under protocol A17019, mouse and guinea pig work at Emory University were approved by the Emory IACUC under protocol numbers DAR-2003089-ENTRPR-N and DAR-2002738-ELMNTS-A, respectively, and mouse studies with

595 HPAIV at the University of Georgia were approved by the UGA IACUC under protocol number A2017

596 05-009.

Acknowledgements

We thank A.Mehle and S.Schultz-Cherry for IAV H5N1 and H7N9 minigenome reporter systems, K.K.Conzelmann for the BSR-T7/5 cell line, C.Jones, S.Johnson, and C.Kyriakis for assistance with the murine HPAIV studies, G.P.Reddy, J.Marlow, and J.DeBergh for assistance with bioanalytical analysis, ImQuest BioSciences for assistance with the human DNA polymerase assay, L.Martinez-Sobrido for IBV isolates, R.T.Jacob for IT support, and A.L.Hammond for critical reading of the manuscript. The MScreen software package was kindly provided by the Center for Chemical Genomics of the University of Michigan under a license agreement by the University of Michigan Office of Technology Transfer, JChem was used for structure database management, search and prediction (JChem 6.2, 2014, ChemAxon (http://www.chemaxon.com)), and Marvin was employed for drawing, displaying and characterizing chemical structures, substructures and reactions (Marvin 14.9.22.0, 2014, ChemAxon (http://www.chemaxon.com)). This work was supported, in part, by contracts HDTRA1-15-C-0075 and HHSN272201500008C from DTRA and the NIH/NIAID, respectively (to G.R.P.) and by public health service grants AI119196, AI071002 and HD079327 from the NIH/NIAID and NIH/NICHD, respectively (to R.K.P.). The funders had no role in study design, data collection and interpretation, or the decision to submit the work for publication.

Competing interests: The authors declare no competing interests.

615 **References**

616 1. Zhou H, Thompson WW, Viboud CG, Ringholz CM, Cheng PY, Steiner C, Abedi GR, Anderson
617 LJ, Brammer L, Shay DK. 2012. Hospitalizations associated with influenza and respiratory
618 syncytial virus in the United States, 1993-2008. Clin Infect Dis 54:1427-36.
619 2. Falsey AR, Hennessey PA, Formica MA, Cox C, Walsh EE. 2005. Respiratory syncytial virus
620 infection in elderly and high-risk adults. N Engl J Med 352:1749-59.
621 3. Thompson WW, Shay DK, Weintraub E, Brammer L, Cox N, Anderson LJ, Fukuda K. 2003.
622 Mortality associated with influenza and respiratory syncytial virus in the United States. JAMA
623 289:179-86.
624 4. Stiver G. 2003. The treatment of influenza with antiviral drugs. CMAJ 168:49-56.
625 5. Skowronski DM, Chambers C, De Serres G, Dickinson JA, Winter A-L, Hickman R, Chan T,
626 Jassem AN, Drews SJ, Charest H, Gubbay JB, Bastien N, Li Y, Krajden M. 2018. Early season
627 co-circulation of influenza A(H3N2) and B(Yamagata): interim estimates of 2017/18 vaccine
628 effectiveness, Canada, January 2018. Euro Surveill 23:pii=18-00035.
629 6. Broor S, Parveen S, Bharaj P, Prasad VS, Srinivasulu KN, Sumanth KM, Kapoor SK, Fowler K,
630 Sullender WM. 2007. A prospective three-year cohort study of the epidemiology and virology of
631 acute respiratory infections of children in rural India. PLoS One 2:e491.
632 7. Mahadevia PJ, Makari D, Masaquel A. 2012. Methodological concerns regarding cost-
633 effectiveness analysis of palivizumab in Florida Medicaid. Arch Pediatr Adolesc Med 166:968-9;
634 author reply 969-70.
635 8. Mahadevia PJ, Masaquel AS, Polak MJ, Weiner LB. 2012. Cost utility of palivizumab
636 prophylaxis among pre-term infants in the United States: a national policy perspective. J Med
637 Econ 15:987-96.
638 9. Weiner LB, Masaquel AS, Polak MJ, Mahadevia PJ. 2012. Cost-effectiveness analysis of
639 palivizumab among pre-term infant populations covered by Medicaid in the United States. J Med
640 Econ 15:997-1018.

641 10. Kamal-Bahl S, Doshi J, Campbell J. 2002. Economic analyses of respiratory syncytial virus
642 immunoprophylaxis in high-risk infants: a systematic review. Arch Pediatr Adolesc Med
643 156:1034-41.
644 11. Hampp C, Kauf TL, Saidi AS, Winterstein AG. 2011. Cost-effectiveness of respiratory syncytial
645 virus prophylaxis in various indications. Arch Pediatr Adolesc Med 165:498-505.
646 12. DeVincenzo JP, El Saleeby CM, Bush AJ. 2005. Respiratory syncytial virus load predicts
647 disease severity in previously healthy infants. J Infect Dis 191:1861-8.
648 13. El Saleeby CM, Bush AJ, Harrison LM, Aitken JA, Devincenzo JP. 2011. Respiratory syncytial
649 virus load, viral dynamics, and disease severity in previously healthy naturally infected children.
650 J Infect Dis 204:996-1002.
651 14. Fiore AE, Fry A, Shay D, Gubareva L, Bresee JS, Uyeki TM, Centers for Disease C, Prevention.
652 2011. Antiviral agents for the treatment and chemoprophylaxis of influenza --- recommendations
653 of the Advisory Committee on Immunization Practices (ACIP). MMWR Recomm Rep 60:1-24.
654 15. Salerno D, Hasham MG, Marshall R, Garriga J, Tsygankov AY, Grana X. 2007. Direct inhibition
655 of CDK9 blocks HIV-1 replication without preventing T-cell activation in primary human
656 peripheral blood lymphocytes. Gene 405:65-78.
657 16. Schang LM. 2006. First demonstration of the effectiveness of inhibitors of cellular protein
658 kinases in antiviral therapy. Expert Rev Anti Infect Ther 4:953-6.
659 17. Prussia A, Thepchatri P, Snyder JP, Plemper RK. 2011. Systematic Approaches towards the
660 Development of Host-Directed Antiviral Therapeutics. Int J Mol Sci 12:4027-52.
661 18. Kaufmann SHE, Dorhoi A, Hotchkiss RS, Bartenschlager R. 2017. Host-directed therapies for
662 bacterial and viral infections. Nat Rev Drug Discov doi:10.1038/nrd.2017.162.
663 19. Shaw ML. 2017. The Next Wave of Influenza Drugs. ACS Infect Dis 3:691-694.
664 20. Dahlin JL, Walters MA. 2014. The essential roles of chemistry in high-throughput screening
665 triage. Future Med Chem 6:1265-90.

21. Baell J, Walters MA. 2014. Chemistry: Chemical con artists foil drug discovery. Nature 513:481-3.

22. Baell JB, Holloway GA. 2010. New substructure filters for removal of pan assay interference compounds (PAINS) from screening libraries and for their exclusion in bioassays. J Med Chem 53:2719-40.

23. Webster RG, Govorkova EA. 2014. Continuing challenges in influenza. Ann N Y Acad Sci 1323:115-39.

24. Voss ME, Carter PH, Tebben AJ, Scherle PA, Brown GD, Thompson LA, Xu M, Lo YC, Yang G, Liu RQ, Strzemienski P, Everlof JG, Trzaskos JM, Decicco CP. 2003. Both 5-arylidene-2-thioxodihydropyrimidine-4,6(1H,5H)-diones and 3-thioxo-2,3-dihydro-1H-imidazo[1,5-a]indol-1-ones are light-dependent tumor necrosis factor-alpha antagonists. Bioorg Med Chem Lett 13:533-8.

25. Anderson LJ, Parker RA, Strikas RL. 1990. Association between respiratory syncytial virus outbreaks and lower respiratory tract deaths of infants and young children. J Infect Dis 161:640-6.

26. Groothuis JR, Woodin KA, Katz R, Robertson AD, McBride JT, Hall CB, McWilliams BC, Lauer BA. 1990. Early ribavirin treatment of respiratory syncytial viral infection in high-risk children. J Pediatr 117:792-8.

27. Anonymous. Ministry of Health, Welfare and Labor, Japan. Summary of media conference by Tamura Ministry of Health, Welfare and Labor, on August 15, 2014 [in Japanese]. http://www.mhlw.go.jp/stf/kaiken/daijin/ 0000054819.html. .

28. DeVincenzo J, Fathi H, Mcclure M, Westland C, Chanda S, Lambkin-Williams R, Smith P, Harrison L, Symons J, Scaglioni-Weinlich C, Zhang Q, Nieforth K, Beigelman L, Blatt L, Fry J. 2014. Treatment with Oral ALS-008176, a Nucleoside Analog, Rapidly Reduces RSV Viral Load and Clinical Disease Severity in a Healthy Volunteer Challenge Study. Open Forum Infectious Diseases Volume 1:Pp. S66-S69.

692 29. Deval J, Hong J, Wang G, Taylor J, Smith LK, Fung A, Stevens SK, Liu H, Jin Z, Dyatkina N,
693 Prhavc M, Stoycheva AD, Serebryany V, Liu J, Smith DB, Tam Y, Zhang Q, Moore ML, Fearns
694 R, Chanda SM, Blatt LM, Symons JA, Beigelman L. 2015. Molecular Basis for the Selective
695 Inhibition of Respiratory Syncytial Virus RNA Polymerase by 2'-Fluoro-4'-Chloromethyl-Cytidine
696 Triphosphate. PLoS Pathog 11:e1004995.
697 30. Yan D, Weisshaar M, Lamb K, Chung HK, Lin MZ, Plemper RK. 2015. Replication-Competent
698 Influenza Virus and Respiratory Syncytial Virus Luciferase Reporter Strains Engineered for Co-
699 Infections Identify Antiviral Compounds in Combination Screens. Biochemistry 54:5589-604.
700 31. Jimenez-Somarribas A, Mao S, Yoon JJ, Weisshaar M, Cox RM, Marengo JR, Mitchell DG,
701 Morehouse ZP, Yan D, Solis I, Liotta DC, Natchus MG, Plemper RK. 2017. Identification of Non-
702 Nucleoside Inhibitors of the Respiratory Syncytial Virus Polymerase Complex. J Med Chem
703 60:2305-2325.
704 32. Weisshaar M, Cox R, Morehouse Z, Kumar Kyasa S, Yan D, Oberacker P, Mao S, Golden JE,
705 Lowen AC, Natchus MG, Plemper RK. 2016. Identification and Characterization of Influenza
706 Virus Entry Inhibitors through Dual Myxovirus High-Throughput Screening. J Virol 90:7368-87.
707 33. Hoffmann HH, Kunz A, Simon VA, Palese P, Shaw ML. 2011. Broad-spectrum antiviral that
708 interferes with de novo pyrimidine biosynthesis. Proc Natl Acad Sci U S A 108:5777-82.
709 34. Krumm SA, Ndungu JM, Yoon JJ, Dochow M, Sun A, Natchus M, Snyder JP, Plemper RK.
710 2011. Potent host-directed small-molecule inhibitors of myxovirus RNA-dependent RNA-
711 polymerases. PLoS One 6:e20069.
712 35. Paul Glezen W, Schmier JK, Kuehn CM, Ryan KJ, Oxford J. 2013. The burden of influenza B: a
713 structured literature review. Am J Public Health 103:e43-51.
714 36. Urakova N, Kuznetsova V, Crossman DK, Sokratian A, Guthrie DB, Kolykhalov AA, Lockwood
715 MA, Natchus MG, Crowley MR, Painter GR, Frolova EI, Frolov I. 2017. beta-D-N(4)-
716 hydroxycytidine is a potent anti-alphavirus compound that induces high level of mutations in
717 viral genome. J Virol doi:10.1128/JVI.01965-17.

718 37. Ehteshami M, Tao S, Zandi K, Hsiao HM, Jiang Y, Hammond E, Amblard F, Russell OO, Merits
719 A, Schinazi RF. 2017. Characterization of beta-d-N(4)-Hydroxycytidine as a Novel Inhibitor of
720 Chikungunya Virus. Antimicrob Agents Chemother 61.
721 38. Hollecker L, Choo H, Chong Y, Chu CK, Lostia S, McBrayer TR, Stuyver LJ, Mason JC, Du J,
722 Rachakonda S, Shi J, Schinazi RF, Watanabe KA. 2004. Synthesis of beta-enantiomers of N4-
723 hydroxy-3'-deoxypyrimidine nucleosides and their evaluation against bovine viral diarrhoea virus
724 and hepatitis C virus in cell culture. Antivir Chem Chemother 15:43-55.
725 39. Barnard DL, Hubbard VD, Burton J, Smee DF, Morrey JD, Otto MJ, Sidwell RW. 2004. Inhibition
726 of severe acute respiratory syndrome-associated coronavirus (SARSCoV) by calpain inhibitors
727 and beta-D-N4-hydroxycytidine. Antivir Chem Chemother 15:15-22.
728 40. Noton SL, Deflube LR, Tremaglio CZ, Fearns R. 2012. The respiratory syncytial virus
729 polymerase has multiple RNA synthesis activities at the promoter. PLoS Pathog 8:e1002980.
730 41. Les A, Adamowicz L, Rode W. 1993. Structure and conformation of N4-hydroxycytosine and
731 N4-hydroxy-5-fluorocytosine. A theoretical ab initio study. Biochim Biophys Acta 1173:39-48.
732 42. Crotty S, Cameron CE, Andino R. 2001. RNA virus error catastrophe: direct molecular test by
733 using ribavirin. Proc Natl Acad Sci U S A 98:6895-900.
734 43. Stuyver LJ, Whitaker T, McBrayer TR, Hernandez-Santiago BI, Lostia S, Tharnish PM, Ramesh
735 M, Chu CK, Jordan R, Shi J, Rachakonda S, Watanabe KA, Otto MJ, Schinazi RF. 2003.
736 Ribonucleoside analogue that blocks replication of bovine viral diarrhea and hepatitis C viruses
737 in culture. Antimicrob Agents Chemother 47:244-54.
738 44. Moore ML, Chi MH, Luongo C, Lukacs NW, Polosukhin VV, Huckabee MM, Newcomb DC,
739 Buchholz UJ, Crowe JE, Jr., Goleniewska K, Williams JV, Collins PL, Peebles RS, Jr. 2009. A
740 chimeric A2 strain of respiratory syncytial virus (RSV) with the fusion protein of RSV strain line
741 19 exhibits enhanced viral load, mucus, and airway dysfunction. J Virol 83:4185-94.
742 45. Chockalingam AK, Hamed S, Goodwin DG, Rosenzweig BA, Pang E, Boyne MT, 2nd, Patel V.
743 2016. The Effect of Oseltamivir on the Disease Progression of Lethal Influenza A Virus

Infection: Plasma Cytokine and miRNA Responses in a Mouse Model. Dis Markers 2016:9296457.

46. Yen HL, Aldridge JR, Boon AC, Ilyushina NA, Salomon R, Hulse-Post DJ, Marjuki H, Franks J, Boltz DA, Bush D, Lipatov AS, Webby RJ, Rehg JE, Webster RG. 2009. Changes in H5N1 influenza virus hemagglutinin receptor binding domain affect systemic spread. Proc Natl Acad Sci U S A 106:286-91.

47. Bouvier NM, Lowen AC. 2010. Animal Models for Influenza Virus Pathogenesis and Transmission. Viruses 2:1530-1563.

48. Lowen AC, Mubareka S, Tumpey TM, Garcia-Sastre A, Palese P. 2006. The guinea pig as a transmission model for human influenza viruses. Proc Natl Acad Sci U S A 103:9988-92.

49. Baranovich T, Wong SS, Armstrong J, Marjuki H, Webby RJ, Webster RG, Govorkova EA. 2013. T-705 (favipiravir) induces lethal mutagenesis in influenza A H1N1 viruses in vitro. J Virol 87:3741-51.

50. Crotty S, Maag D, Arnold JJ, Zhong W, Lau JY, Hong Z, Andino R, Cameron CE. 2000. The broad-spectrum antiviral ribonucleoside ribavirin is an RNA virus mutagen. Nat Med 6:1375-9.

51. Banks GR, Brown DM, Streeter DG, Grossman L. 1971. Mutagenic anologues of cytosine: RNA polymerase template and substrate studies. J Mol Biol 60:425-39.

52. Budowsky EI, Sverdlov ED, Monastyrskaya GS. 1972. New method of selective and rapid modification of the cytidine residues. FEBS Lett 25:201-204.

53. Traut TW. 1994. Physiological concentrations of purines and pyrimidines. Mol Cell Biochem 140:1-22.

54. Lauring AS, Frydman J, Andino R. 2013. The role of mutational robustness in RNA virus evolution. Nat Rev Microbiol 11:327-36.

55. Crotty S, Andino R. 2002. Implications of high RNA virus mutation rates: lethal mutagenesis and the antiviral drug ribavirin. Microbes Infect 4:1301-7.

769 56. Pauly MD, Lauring AS. 2015. Effective lethal mutagenesis of influenza virus by three nucleoside
770 analogs. J Virol 89:3584-97.
771 57. Jin Z, Smith LK, Rajwanshi VK, Kim B, Deval J. 2013. The ambiguous base-pairing and high
772 substrate efficiency of T-705 (Favipiravir) Ribofuranosyl 5'-triphosphate towards influenza A
773 virus polymerase. PLoS One 8:e68347.
774 58. Graci JD, Cameron CE. 2006. Mechanisms of action of ribavirin against distinct viruses. Rev
775 Med Virol 16:37-48.
776 59. Salganik RI, Vasjunina EA, Poslovina AS, Andreeva IS. 1973. Mutagenic action of N4-
777 hydroxycytidine on Escherichia coli B cyt. Mutat Res 20:1-5.
778 60. Jakobs HH, Froriep D, Havemeyer A, Mendel RR, Bittner F, Clement B. 2014. The
779 mitochondrial amidoxime reducing component (mARC): involvement in metabolic reduction of
780 N-oxides, oximes and N-hydroxyamidinohydrazones. ChemMedChem 9:2381-7.
781 61. Janion C. 1984. Some problems of mutagenesis induced by base analogues. Acta Biochim Pol
782 31:183-92.
783 62. Yan D, Lee S, Thakkar VD, Luo M, Moore ML, Plemper RK. 2014. Cross-resistance mechanism
784 of respiratory syncytial virus against structurally diverse entry inhibitors. Proc Natl Acad Sci U S
785 A 111:E3441-9.
786 63. Krumm SA, Yan D, Hovingh ES, Evers TJ, Enkirch T, Reddy GP, Sun A, Saindane MT,
787 Arrendale RF, Painter G, Liotta DC, Natchus MG, von Messling V, Plemper RK. 2014. An orally
788 available, small-molecule polymerase inhibitor shows efficacy against a lethal morbillivirus
789 infection in a large animal model. Sci Transl Med 6:232ra52.
790 64. Bright RA, Shay D, Bresee J, Klimov A, Cox N, Ortiz J, Ctr WC, CDC. 2006. High levels of
791 adamantane resistance among influenza A (H3N2) viruses and interim guidelines for use of
792 antiviral agents - United States, 2005-06 influenza season (Reprinted from MMWR, vol 55, pg
793 44-46, 2006). Jama-Journal of the American Medical Association 295:881-882.

65. Okomo-Adhiambo M, Nguyen HT, Abd Elal A, Sleeman K, Fry AM, Gubareva LV. 2014. Drug susceptibility surveillance of influenza viruses circulating in the United States in 2011-2012: application of the WHO antiviral working group criteria. Influenza Other Respir Viruses 8:258-65.

66. Marjuki H, Mishin VP, Chesnokov AP, Jones J, De La Cruz JA, Sleeman K, Tamura D, Nguyen HT, Wu HS, Chang FY, Liu MT, Fry AM, Cox NJ, Villanueva JM, Davis CT, Gubareva LV. 2014. Characterization of Drug-Resistant Influenza A(H7N9) Variants Isolated From an Oseltamivir-Treated Patient in Taiwan. J Infect Dis doi:10.1093/infdis/jiu447.

67. Nguyen HT, Fry AM, Gubareva LV. 2012. Neuraminidase inhibitor resistance in influenza viruses and laboratory testing methods. Antivir Ther 17:159-73.

68. McKimm-Breschkin JL, Williams J, Barrett S, Jachno K, McDonald M, Mohr PG, Saito T, Tashiro M. 2013. Reduced susceptibility to all neuraminidase inhibitors of influenza H1N1 viruses with haemagglutinin mutations and mutations in non-conserved residues of the neuraminidase. J Antimicrob Chemother 68:2210-21.

69. McKimm-Breschkin JL. 2013. Influenza neuraminidase inhibitors: antiviral action and mechanisms of resistance. Influenza Other Respir Viruses 7 Suppl 1:25-36.

70. Stokes KL, Chi MH, Sakamoto K, Newcomb DC, Currier MG, Huckabee MM, Lee S, Goleniewska K, Pretto C, Williams JV, Hotard A, Sherrill TP, Peebles RS, Jr., Moore ML. 2011. Differential pathogenesis of respiratory syncytial virus clinical isolates in BALB/c mice. J Virol 85:5782-93.

71. Peebles RS, Jr., Graham BS. 2005. Pathogenesis of respiratory syncytial virus infection in the murine model. Proc Am Thorac Soc 2:110-5.

72. Belser JA, Wadford DA, Pappas C, Gustin KM, Maines TR, Pearce MB, Zeng H, Swayne DE, Pantin-Jackwood M, Katz JM, Tumpey TM. 2010. Pathogenesis of pandemic influenza A (H1N1) and triple-reassortant swine influenza A (H1) viruses in mice. J Virol 84:4194-203.

73. Belser JA, Lu X, Maines TR, Smith C, Li Y, Donis RO, Katz JM, Tumpey TM. 2007. Pathogenesis of avian influenza (H7) virus infection in mice and ferrets: enhanced virulence of Eurasian H7N7 viruses isolated from humans. J Virol 81:11139-47.

74. Yang YT, Evans CA. 1961. Hypothermia in mice due to influenza virus infection. Proc Soc Exp Biol Med 108:776-80.

75. Sudo K, Watanabe W, Mori S, Konno K, Shigeta S, Yokota T. 1999. Mouse model of respiratory syncytial virus infection to evaluate antiviral activity in vivo. Antivir Chem Chemother 10:135-9.

76. Mok CK, Lee HH, Chan MC, Sia SF, Lestra M, Nicholls JM, Zhu H, Guan Y, Peiris JM. 2013. Pathogenicity of the novel A/H7N9 influenza virus in mice. MBio 4.

77. Kang YM, Song BM, Lee JS, Kim HS, Seo SH. 2011. Pandemic H1N1 influenza virus causes a stronger inflammatory response than seasonal H1N1 influenza virus in ferrets. Arch Virol 156:759-67.

78. Hayden FG, Fritz R, Lobo MC, Alvord W, Strober W, Straus SE. 1998. Local and systemic cytokine responses during experimental human influenza A virus infection. Relation to symptom formation and host defense. J Clin Invest 101:643-9.

79. Paquette SG, Banner D, Zhao Z, Fang Y, Huang SS, Leomicronn AJ, Ng DC, Almansa R, Martin-Loeches I, Ramirez P, Socias L, Loza A, Blanco J, Sansonetti P, Rello J, Andaluz D, Shum B, Rubino S, de Lejarazu RO, Tran D, Delogu G, Fadda G, Krajden S, Rubin BB, Bermejo-Martin JF, Kelvin AA, Kelvin DJ. 2012. Interleukin-6 is a potential biomarker for severe pandemic H1N1 influenza A infection. PLoS One 7:e38214.

80. Killian ML. 2008. Hemagglutination assay for the avian influenza virus. Methods Mol Biol 436:47-52.

81. Razinkov V, Huntley C, Ellestad G, Krishnamurthy G. 2002. RSV entry inhibitors block F-protein mediated fusion with model membranes. Antiviral Res 55:189-200.

Table 1. NHC efficacy against a panel of influenza virus and RSV isolates. Potency of NHC against different IAVs, IBVs, and RSVs determined in cultured cells or embryonated chicken eggs. IAVs are sorted by lineage and subtype. EC_{50} values were determined through four-parameter variable slope regression modeling, 95% confidence intervals in brackets.

Viral Strain	Assay Method; Host System	EC_{50} [μM]	SI	Origin
A/WSN/33 (H1N1)	Plaque assay, MDCK cells	3.1 [2.25-3.82]	98	Human
A/WSN/33 (H1N1)	$TCID_{50}$-HA assay, MDCK cells	1.1 [0.86-1.22]	275	Human
A/California/7/2009 (H1N1) pdm09	$TCID_{50}$-HA assay, MDCK cells	3.1 [1.49-6.23]	98	Human pdm09
A/Georgia/M5081/2012 (H1N1)	$TCID_{50}$-HA assay, MDCK cells	3.4 [2.92-3.9]	89	Human pdm09
A/Netherlands/602/2009 (H1N1) pdm09	$TCID_{50}$-HA assay, MDCK cells	1.8 [1.17-2.55]	171	Human pdm09
A/duck/Alberta/35/76 (H1N1)	HA assay, *in ovo*	0.6 [0.45-0.48]	N/A	Avian
A/swine/Spain/53207/2004 (H1N1)	HA assay, *in ovo*	0.1 [0.02-0.12]	N/A	Swine; Eurasian Avian-like
A/chicken/Potsdam/178-4/83 (H2N2)	HA assay, *in ovo*	0.4 [0.15-1.35]	N/A	Avian
A/Vietnam/1203/2004(H5N1)	$TCID_{50}$, MDCK cells	0.14	2143	Avian
A/Anhui/1/2013(H7N9)	$TCID_{50}$, MDCK cells	0.13	2308	Avian
A/Aichi/2/68 (H3N2)	$TCID_{50}$-HA assay, MDCK cells	3.2 [2.68-3.88]	93	Human
A/Wisconsin/67/2005 (H3N2)	$TCID_{50}$-HA assay, MDCK cells	1.7 [1.27-2.33]	182	Human
A/Panama/2007/99 (H3N2)	$TCID_{50}$-HA assay, MDCK cells	1.2 [0.05-2.0]	250	Human
A/swine/Ohio/sw10-132/2010 (H3N2)	$TCID_{50}$-HA assay, MDCK cells	3.2 [2.52-4.05]	95	Swine; triple reassortant lineage
B/Yamagata/16/88	$TCID_{50}$, MDCK cells	0.015 [0.011-0.019]	20,000	Human
B/Brisbane/60/08	$TCID_{50}$, MDCK cells	0.006 [0.003-0.008]	50,000	Human
recRSV-A2-L19F	Reporter-assay, Hep2 cells	3.7 [2.8-4.9]	74	Human
RSV clinical strain 5S9	Plaque assay, Hep2 cells	0.69 [0.5-0.9]	394	Human
RSV clinical strain 718	Plaque assay, Hep2 cells	0.51 [0.4-0.7]	533	Human

Table 2. Quantitation of transition mutations in NHC-experienced viral RNA. Summary of the mutation frequency analysis in viral RNA after 24-hour exposure of IAV-WSN or RSV-A2-L19F infected cells to 10 μM NHC.

IAV-WSN	Total nt.	C to U	G to A	A to G
10 μM NHC	7737	22	21	2
DMSO	12539	2	3	4
% nt. content	A – 34.4%	T – 23.3%	G - 22.4%	C – 19.9%

RSV-A2	Total nt.	C to U	G to A	A to G
10 μM NHC	9836	5	6	9
DMSO	10971	0	0	2
% nt. content	A – 37.4%	T – 33.3%	G - 14.6%	C – 14.6%

Table 3. Calculation of PK parameters for NHC after a single i.p. or p.o. dose of mice. Parameters and dose-dependent oral bioavailability of NHC were calculated using the WinNonlin (Pharsight) software package.

Route	Dose [mg/kg]	T_{max} [hours]	C_{max} [nmol/ml]	AUC (0-∞) [hr*nmol/ml]	Vz-F [L/kg]	Cl-F [L/hr/kg]	T(1/2) [hours]	Bioavailability (%)
I.P.	10	0.25	10.5	9.8	16	3.9	2.8	N/A
I.P.	50	0.08	70.4	62	22.7	3.1	5	N/A
p.o.	50	0.5	30.2	31.4	45.8	6.1	5.2	56
p.o.	150	1	31.4	71	37.9	8.2	3.2	43
p.o.	500	0.5	47.2	202.9	36.8	9.5	2.7	36

858 **Figure legends:**

859 **Fig. 1** Ribonucleoside analog NHC blocks negative-strand RNA viruses associated with influenza-like
860 diseases. **A)** Simultaneous anti-RSV and anti-IAV screen of a ribonucleoside analog library, carried out
861 in triplicate. Shown are individual biological replicates (grey symbols) and mean values (black lines) ±
862 SD. Hit candidates are highlighted in color, hit cut-off ≥ 80% inhibition. **B)** Structure of the NHC hit
863 candidate. For all dose-response measurements shown in **C-G**, symbols represent means ± SD of at
864 least three biological repeats, expressed relative to vehicle (DMSO)-treated controls. EC_{50} and CC_{50}
865 concentrations were calculated through four-parameter variable slope regression modeling, 95%
866 confidence intervals in brackets. **C)** NHC activity against two RSV isolates on HEp-2 cells. Virus
867 titration through plaque assay. PrestoBlue reagent was used to determine the effect of treatment on cell
868 metabolic activity. **D)** NHC activity against viruses representing group 1 and 2 HAs on MDCK cells.
869 Virus titration through $TCID_{50}$-HA assays. **E)** Efficacy of NHC against an HPAIV and an emerging AIV
870 subtype on MDCK cells. Virus titration through plaque assay. **F)** Efficacy of NHC against IBVs
871 representing both currently circulating lineages on MDCK cells. Virus titration through $TCID_{50}$ assays.
872 **G)** Comparison of NHC and T-705 antiviral efficacy on primary human bronchial tracheal epithelial cells
873 (HBTEC) vs. MDCK cells. Virus replication assessment based on virus-encoded luciferase reporter
874 activity. Analysis with 2-way ANOVA, *P* values are shown (NS not significant).

875 **Fig. 2** Mechanistic assessment of NHC. **A)** Time-of-addition variation assays. MDCK cells (left panel)
876 were infected with IAV-WSN-nanoLuc and treated with 10 µM NHC, 50 µM T-705 (positive control
877 influenza virus RdRp inhibitor (57)) or 10 µM GRP-71271 (positive control IAV-WSN entry inhibitor (32))
878 at different times relative to infection. Hep2 cells (right panel) were infected with recRSV-A2-L19F-
879 fireSMASh and treated with 10 µM NHC, 10 µM ALS-8176 (positive control RSV RdRp inhibitor (29)) or
880 10 µM CL-309623 (positive control RSV entry inhibitor (81)) at different times relative to infection.
881 Reporter activity is expressed relative to vehicle-treated control infections (dashed lines). Values
882 represent means of three biological repeats ± SD. **B)** NHC activity in dose-response minigenome

883 assays. 293T cells were transiently transfected with IAV-WSN (H1N1), A/Vietnam (H5N1), A/Anhui
884 (H7N9) or RSV minigenome systems. Increasing concentrations of NHC were added to the cells
885 immediately post-transfection. Luciferase reporter activity was measured after 30-hour exposure and is
886 expressed relative to vehicle-treated wells. Means of three biological repeats ± SD are shown. Analysis
887 through four-parameter variable slope regression modeling. **C)** Effect of NHC-TP on human DNA
888 polymerase α activity. *In vitro* polymerase assays were carried out in the presence of a range of NHC-
889 TP concentration or Alphidicolin for reference. Symbols represent mean values ± SD of 3 biological
890 repeats each. **D)** *In cellula* nucleoside competition assay. MDCK cells infected with WSN-nanoLuc (left
891 panel) or RSV-fireSMASh (right panel) were exposed to 10 μM NHC and increasing concentrations of
892 exogenously added natural nucleosides at the onset of infection. Values were normalized to vehicle-
893 treated controls and show means of three biological repeats ± SD. **E)** *In vitro* RSV RdRp activity assay.
894 Purified RSV P-L complexes were incubated with 25-mer RNA oligonucleotide template and rNTPs
895 (lacking CTP) with [α-^{32}P]-UTP tracer. NHC (green), NHC-TP (red), or CTP (black) were added at the
896 specified final concentrations. Controls lacked CTP or contained inactive L_{D811A} mutant. Lengths of the
897 reaction products were determined using Tr 1-25 and Tr 3-25 standards, the sequence of the
898 predominant 23-mer amplicon originating from major initiation at the +3 position is shown on the right.
899 **F)** Transition mutation frequency in viral RNA. Total RNA was extracted from cells infected with WSN
900 (top panel) or RSV (bottom panel) in the presence of 10 μM NHC or vehicle. Treatment was started
901 immediately at the time of infection. PB1- or L-encoding cDNA was subcloned and at least 10
902 independent clones each subjected to Sanger sequencing; at least 7,737 nucleotides were determined
903 per virus and exposure condition. Statistical analysis with Fisher's exact test.
904 **Fig. 3** Anabolism and PK/PD profiling of NHC. **A)** Anabolism of NHC in primary HBTECs. Cells were
905 incubated with 20 μM NHC for the indicated exposure times and intracellular concentrations of NHC
906 and anabolites (NHC-5'-monophosphate (NHC-MP) and NHC-TP) determined through LC/MS/MS. **B)**
907 NHC anabolite stability in HBTECs. Cells grown in the presence of 20 μM NHC for 24 hours were

908 switched to drug-free media and anabolite concentrations monitored over a 6-hour period through
909 LC/MS/MS. **C, D)** Time-concentration profiles for plasma levels of NHC after a single I.P. (C) or oral (D)
910 dose of mice (3 animals per time point) at the specified levels. PK/PD profiles after a single oral dose of
911 mice (3 animals per time point) at the specified levels. **E, F)** Lung tissue concentrations of NHC (E) and
912 of the bioactive NHC-TP anabolite (F) after a single oral NHC dose at the specified levels. Samples in
913 A-F were analyzed through LC/MS/MS and symbols represent mean values ± SD of 3 biological
914 repeats each.

915 **Fig. 4** *In vivo* efficacy of NHC. For experiments shown in **A-F**, BALB/cJ mice were infected i.n. with
916 1×10^5 pfu of RSV-A2-L19F (A, B) or 1,000 pfu of IAV-PR8 (C-F) and NHC dosed orally b.i.d. Symbols
917 represent individual biological repeats, columns show mean values ± SD; LOD limit of detection. **A)**
918 Lung RSV loads were determined five days post-infection through immunoplaque assays. Dosing was
919 initiated prophylactically two hours pre-infection. 1-way ANOVA with Tukey's post hoc test. **B)** Breath
920 distension of peripheral arteries was quantified eight days post-infection with RSV through pulse
921 oximetry. Control animals were mock-infected and vehicle treated. 1-way ANOVA with Tukey's post hoc
922 test. **C)** Lung IAV-PR8 loads were determined six days post-infection. Dosing was initiated
923 prophylactically. 1-way ANOVA with Dunnett's post hoc test. **D)** Comparison of NHC with SOC
924 oseltamivir. Lung IAV-PR8 loads were determined on the specified days post-infection. Dosing was
925 initiated prophylactically. 2-way ANOVA with Tukey's post hoc test. **E)** Relative pro-inflammatory
926 cytokines IFN-γ and IL-6 expression levels in lung tissue of IAV-PR8-infected animals were quantified
927 through RT-qPCR three days post-infection and are expressed relative to uninfected, vehicle-treated
928 animals. 1-way ANOVA with Dunnett's post hoc test. **F)** Post-exposure dosing of NHC, initiated six
929 hours post-infection. Lung IAV-PR8 loads were determined three and six days post-infection. Unpaired
930 t-tests with Welch's correction for each time point. **G)** Oral efficacy of NHC against HPAIV. Mice were
931 infected with 6 pfu of A/Vietnam/1203/2004 (H5N1) and brain and lung virus loads determined six days
932 post-infection. Treatment was initiated prophylactically 2 hours pre-infection; 1-way ANOVA with

933 Tukey's post hoc test. **H, I)** Oral NHC efficacy and suppression of virus transmission in guinea pigs.
934 Source animals were infected i.n. with 10^4 pfu of IAV-NL/09 and virus loads in nasal lavages
935 determined on days 1, 3, 5, and 7 post-infection (H). Treatment was initiated prophylactically two hours
936 pre-infection and continued b.i.d. to the end of day 3 post-infection. Untreated and uninfected contact
937 animals were added 24 hours post-infection and transmitted virus titers in nasal lavages determined on
938 days 2, 4, 6, and 8 (I). Analysis with 2-way ANOVA and Dunnett's post hoc test.

Figure 1

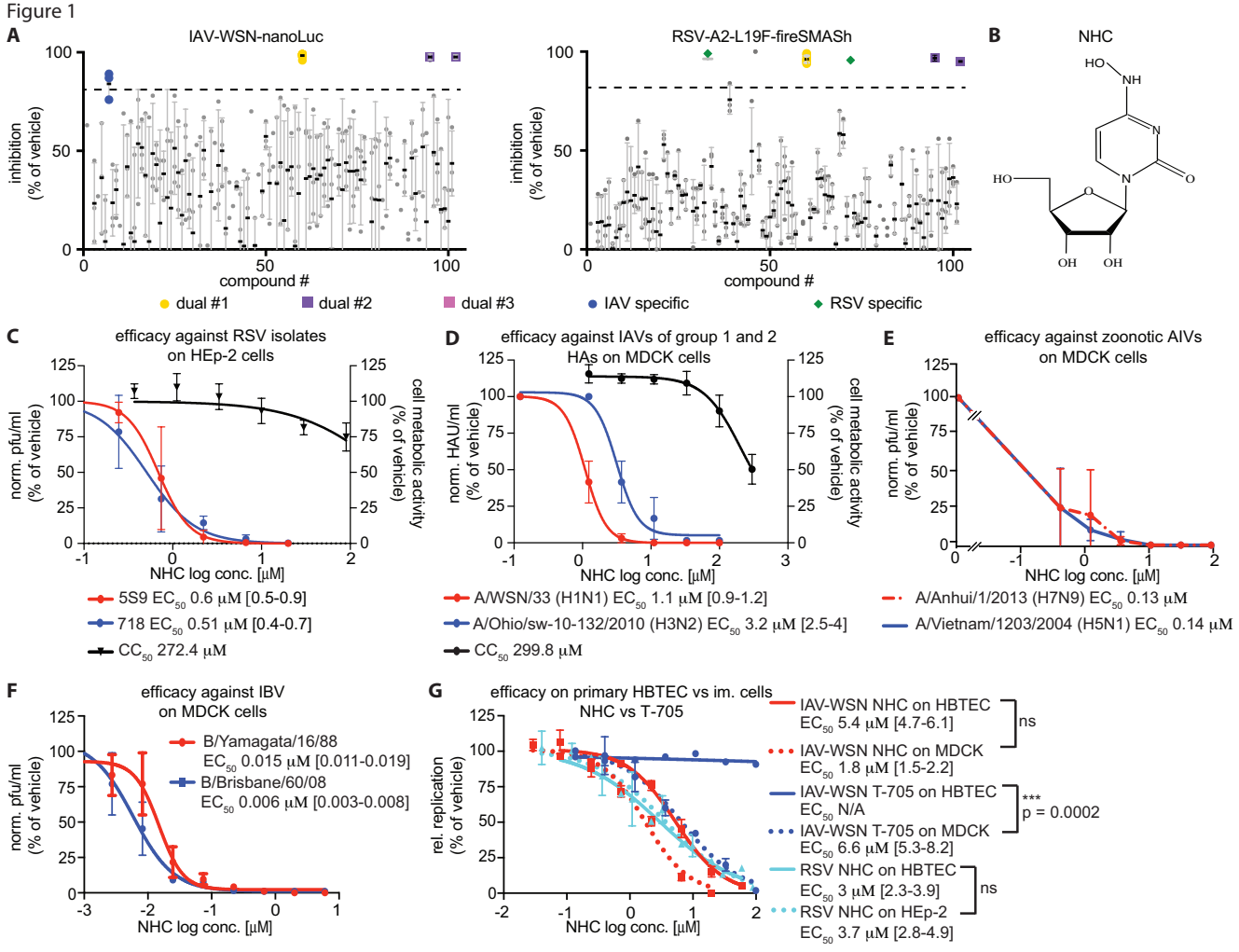

Figure 2

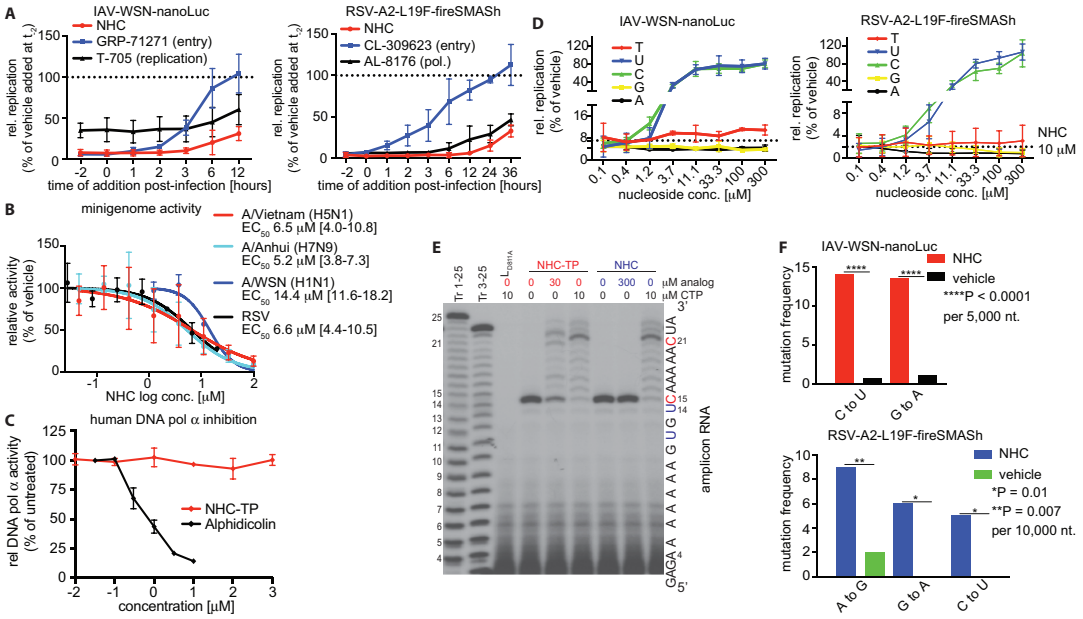

Figure 3

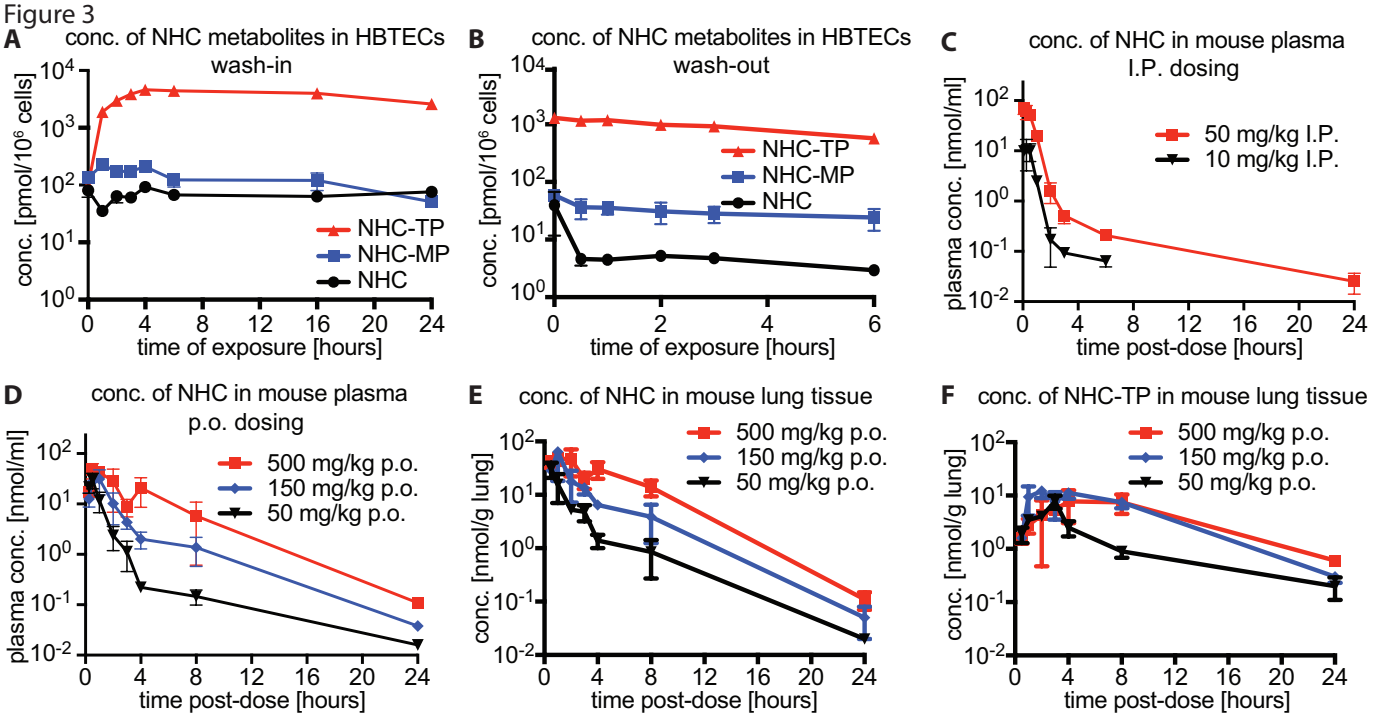

Figure 4